Vasilis Tsourapas
e-mail: djvas@umich.edu

Jing Sun
e-mail: jingsun@umich.edu

Department of Naval Architecture and Marine Engineering,
University of Michigan,
NAME Building,
2600 Draper Road,
Ann Arbor, MI 48109-2145

Anna Stefanopoulou
Department of Mechanical Engineering,
W. E. Lay Automotive Laboratory,
University of Michigan,
1231 Beal Avenue,
Room 2043,
Ann Arbor, MI 48109-2121
e-mail: annastef@umich.edu

Control Oriented Analysis of a Hybrid Solid Oxide Fuel Cell and Gas Turbine System

The goal of this work is to investigate the feasibility of a hybrid solid oxide fuel cell (SOFC) and gas turbine (GT) system for mobile power production. A system consisting of a gas turbine, a burner, and an SOFC is examined to gain fundamental understanding of the system dynamics. A control oriented dynamic model is developed to provide the critically needed tool for system feasibility analysis and control strategy design. System optimization and transient analysis are performed based on the system model to determine the desired operating conditions and load following limitations. It is shown that the open loop system will shut down in the case of a large load step. Based on the insights learned from the open loop analysis, a feedback control scheme is proposed. The feedback scheme is based on a reference governor, which modifies the load applied to the generator to guarantee stability and fast tracking during transients.
[DOI: 10.1115/1.3081467]

1 Introduction

Integrating fuel cell based power systems with energy recuperation devices (ERDs) can improve the system efficiency by minimizing the exhaust energy losses. A conceptual schematic diagram of an integrated fuel cell system with energy recuperation devices is shown in Fig. 1. For fuel cell power systems, there are several special reasons that make the energy recuperation particularly attractive. In order to promote the fuel cell efficiency and avoid hydrogen starvation issues, fuel cell stacks do not operate at fuel utilization ratios close to 100% [1–3]. Thus, a portion of the fuel provided to the fuel cell will be wasted unless energy recuperation devices are incorporated. Significant amounts of energy can be recovered by utilizing the remaining hydrogen in the exhaust, given the high heating value of hydrogen. For the high temperature solid oxide fuel cells (SOFCs), especially for the pressurized SOFCs, the high exhaust temperature and energy content make the energy recuperation even more appealing. The main devices used to facilitate energy recuperation from SOFC systems are catalytic burners, gas turbine (GT), and generator combinations, as shown in Fig. 2. Note that the system examined here is intended for mobile applications with no grid power connection. For such applications, the use of energy storage devices and power electronics often allows proper conditioning of the power drawn from the SOFC and the generator. In this work, the goal is to develop a control scheme to meet mobile power demand and to avoid system shutdown without relying on the energy storage devices. The insights gained from this study could be used to understand the limiting performance of the system and to develop guidelines in properly sizing the energy storage device.

The integrated fuel cell systems with energy recuperation devices have been studied extensively in literature, motivated by the substantial benefits of ERDs. Publications focusing on the dynamic behavior and load transitions of hybrid solid oxide fuel cell and gas turbine systems are fewer than the ones focusing on steady state performance in today's literature. Most work done on SOFC/GT systems includes cost and efficiency studies for optimal design and material selection.

A cost versus efficiency analysis in Ref. [4] indicates the increase in system efficiency and reduction in cost when a GT cycle is integrated with an SOFC. Multiple studies show that the steady state efficiency increases when energy recuperation devices are integrated in a fuel cell system [5–7]. Increase in SOFC efficiency is shown by Yi et al. in Ref. [8] when the SOFC operating pressure increases at the expense of capital cost. An efficient and low cost solution for pressurizing the SOFC system is the addition of a GT. Further increase in efficiency is observed by Yang et al. [9] when internal reforming is used. Yang compares SOFC internal and external reforming and states that the advantage of the internal reforming, in terms of efficiency, is more evident in the hybrid systems than in the stand-alone SOFC system due to the higher exhaust temperature (i.e., higher exhaust energy content) and the capability of the system to harvest the exhaust energy. Steady state modeling, optimization, and parametric studies in Refs. [5,10–16] determine the theoretical maximum electrical efficiency of a combined SOFC and GT cycle to be around 60%.

Publications dealing with the transient dynamics of the system (i.e., the system's response to changes in demanded power), though, are fewer. Significant publications on control oriented analysis of SOFC systems, including the balance of plant components [17,18], identify the load following limitations and implement model predictive control schemes to resolve them. On coupled SOFC/GT systems, a dynamic model of an SOFC/GT system is developed in Ref. [19]. The model is validated using startup operation experimental data provided by Siemens Westinghouse and the authors note that the model, built from first principles, can reasonably predict the dynamic performance of a complex hybrid SOFC/GT system. The authors of Ref. [20] developed a dynamic model of an SOFC/GT system and evaluated the matching between that model and a linearized version of the same model. They noted that the linear and nonlinear model responses matched only for small variations (less that 10%) in the inputs. Thus, the nonlinearities cannot be ignored in the system model and performance analysis. In Ref. [21], using dynamic analysis, it is identified that regulating the shaft speed in a SOFC/GT system can be achieved by direct injection of fuel flow in the catalytic

Manuscript received June 15, 2007; final manuscript received August 20, 2008; published online August 12, 2009. Review conducted by Ben Wilhite. Paper presented at the Fifth International Fuel Cell Science Engineering and Technology Conference (FUELCELL2007), Brooklyn, NY, June 18–20, 2007.

Copyright © 2009 by ASME

Downloaded From: http://electrochemical.asmedigitalcollection.asme.org/ on 02/18/2016 Terms of Use: http://www.asme.org/about-asme/terms-of-use

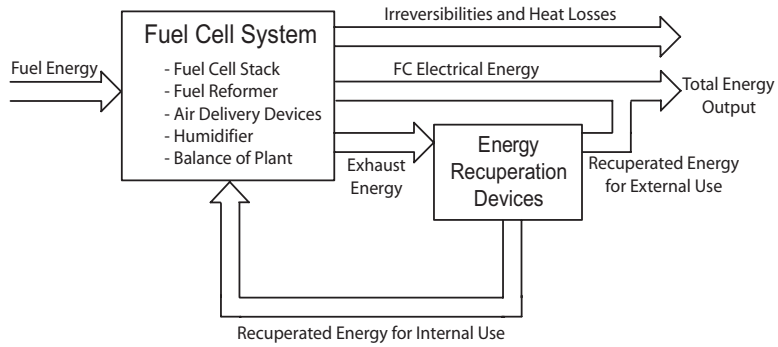

Fig. 1 Energy flow of integrated fuel cell system with energy recuperation devices

burner. Finally, the authors of [22] pointed out that: "With a given constant generator power, the system is at an unstable equilibrium. Departing from steady state, for example, a step increase of the generator power will lead to deceleration of the shaft speed. No new equilibrium will be found within the valid bounds of shaft speed." The authors noted that proper shaft speed regulation can be achieved via "trial-and-error tuning of a PID controller," using as feedback the error between the actual air flow and the air flow setpoint. The system stability, though, is not guaranteed for a load step different than the one the PID controller was tuned for. In this work a reference governor (RG) is implemented in the SOFC/GT system with global convergence properties, and in future work an alternative reference governor, suitable for real-time application, will be presented and combined with direct fuel injection into the catalytic burner (CB).

The focus of this paper is on the efficient steady state operation and transient response of a highly coupled SOFC and gas turbine system. The system and the associated model are described in Sec. 2, while the system efficiency optimization along with its open loop analysis is presented in Sec. 3. In Secs. 3 and 4, the load following limitations of the system are identified, and potential solutions to mitigate them are proposed. Finally, in Sec. 5, a reference governor is integrated into the system to ensure proper load following capabilities.

2 System Operation and Numerical Model

The system investigated, shown in Fig. 2, is rated at 30 kW and is composed of a compressor (C), an SOFC stack, a catalytic burner (CB), and a turbine (T), which drives a generator (GEN). The hybrid SOFC/GT system analyzed in this work is intended as an auxiliary power unit (APU) for military and commercial mobile applications. Other components, such as the reformer and the heat exchangers, are not included in this work in order to focus on the coupling dynamics between the SOFC and the GT. Air is supplied to the cathode side of the SOFC by the compressor, while prereformed fuel is fed to the anode side. The exhaust from the SOFC outlet passes through the CB, where the fuel that has not been utilized in SOFC is burned to increase the temperature of the flow. The flow from the CB then powers the turbine, thereby providing a mechanism to recuperate the exhaust energy. The turbine drives both the compressor and the generator; the former delivers the air needed for the SOFC stack operation and the latter provides additional electrical power for the system. The net power output is the sum of the electric power from the SOFC and the generator. In order to explore the dynamic characteristics of the integrated SOFC/GT system, effort is initially devoted to develop a dynamic model that captures both the steady state and dynamic behavior of the system. This model is presented in Secs. 2.1–2.4.

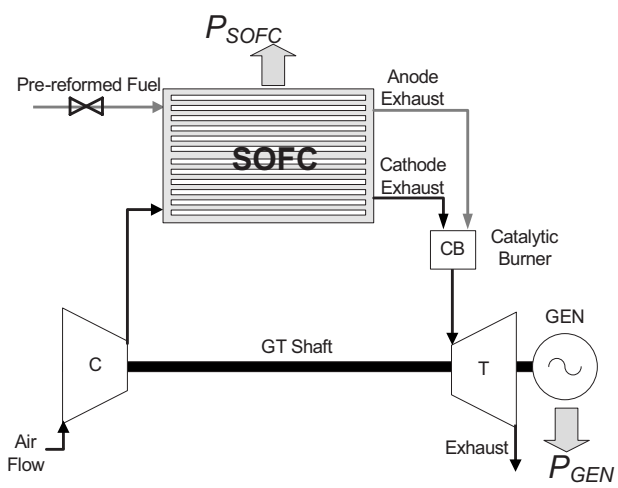

Fig. 2 Schematic of a hybrid SOFC/GT system

2.1 Solid Oxide Fuel Cell Model. The SOFC model utilized in the work was developed by Xi in Ref. [1], where a thorough model-based control analysis was performed, and the issues associated with an SOFC system coupled with a fuel reformer were addressed. It is shown that thermal management and reactant ratio control are required to ensure fast and safe load transitions. An overview of the model is included here for a self-contained system model presentation. In this work a coflow SOFC arrangement is utilized, as illustrated in Fig. 3. The SOFC model is composed of three separate submodels, namely, the electrochemical submodel, the mass balance submodel, and the energy balance submodel. The stack model is then developed by integrating those submodels, as presented in Secs. 2.2–2.4.

Note that in this work the fuel entering the SOFC is assumed to be partially reformed, containing CH_4, CO_2, CO, H_2O, H_2, and N_2, and has the following fixed molar fraction composition:

$$x_f = (x_{CH_4}, x_{CO_2}, x_{CO}, x_{H_2O}, x_{H_2}, x_{N_2}) = (0.016, 0.018, 0.163, 0.037, 0.324, 0.442) \quad (1)$$

while in the air channel, we assume

$$x_a = (x_{O_2}, x_{N_2}) = (0.21, 0.79) \quad (2)$$

In order to capture the spatial distribution of important variables in the SOFC, such as current density and temperature, the model presented in Ref. [1] utilizes the finite-volume method to discretize the cell into a user-defined number of units along the gas flow direction, where the electrode and electrolyte layers are considered as one assembly structure, called the positive electrode-electrolyte-negative electrode (PEN). In one discretization unit, variables such as the current density, temperatures, and pressures are assumed to be homogeneous. Dynamic governing equations for each unit in the SOFC model are derived by apply-

Downloaded From: http://electrochemical.asmedigitalcollection.asme.org/ on 02/18/2016 Terms of Use: http://www.asme.org/about-asme/terms-of-use

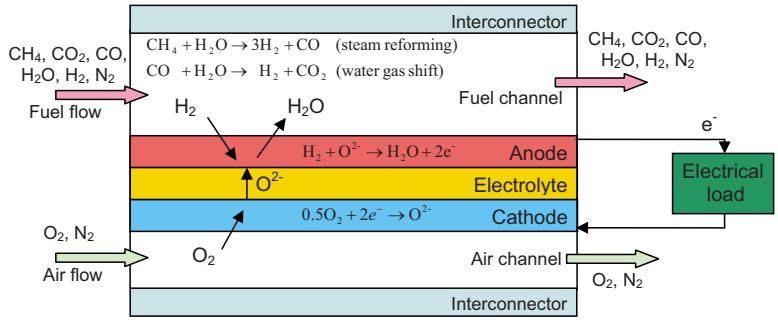

Fig. 3 Operating principle of coflow planar SOFCs [1]

ing the electrochemical, thermal dynamic, and fluid flow principles. These discretization units are then integrated to form the SOFC model by imposing the gas flows, heat exchanges, and current distribution relations.

The operating voltage of one discretization unit of the cell can be calculated by

$$U^j = U^j_{\mathrm{OCV}} - (\eta^j_{\mathrm{ohm}} + \eta^j_{\mathrm{act}} + \eta^j_{\mathrm{con}}) \tag{3}$$

where j is the index of discretization units. U^j_{OCV} is the open circuit voltage, and the last three terms in Eq. (3) represent various potential losses in the jth unit. Note that for notation simplicity the superscript j will be omitted in the following equations. The open circuit voltage can be determined by the Nernst equation. The η_{ohm} term is the ohmic loss due to the internal resistance in the SOFC and the activation loss, η_{act}, is due to the energy barrier to be overcome in order for the electrochemical reaction to occur, and can be characterized by the Butler–Volmer equation. The concentration loss, η_{con}, reflects the overpotential due to the species diffusions between the reaction site and the bulk flow in the gas channels.

Finally, the polarization relation in each discretization unit, as denoted by the following nonlinear algebraic function, can be determined in the electrochemical submodel based on the local conditions, including the PEN temperature and species pressures:

$$U = f(i, p_{\mathrm{H_2}}, p_{\mathrm{O_2}}, p_{\mathrm{H_2O}}, p_a, T_{\mathrm{PEN}}) \tag{4}$$

where details on the expression for the function f are given in Ref. [1]. It is noted that there are no state variables in the electrochemical submodel.

The mass accumulated in the fuel and air channels are calculated in the mass balance submodel. Each discretization unit of the cell has eight state variables, representing the molar concentrations of different gas species, i.e., CH_4, CO_2, CO, H_2O, H_2, and N_2 in the fuel channel, and O_2 and N_2 in the air channel.

In the planar SOFC model, the cell is usually divided into several temperature layers to represent the temperature distribution along the axis perpendicular to the cell plate. In the model presented in Ref. [1], there are five layers, namely, the fuel bulk flow, the air bulk flow, the PEN, the fuel-side interconnector, and the air-side interconnect in each discretization unit of the SOFC. For the cells at the boundaries of the stack, the fuel/air-side interconnectors have to be considered as separate temperature layers in the model.

The temperatures of these layers are calculated by solving the dynamic equations of energy balance in each layer. The heat transfer considered in the model includes the convection between the bulk flows and their surrounding solid structures, the conduction in solid layers, as well as the radiation between PEN, and interconnectors. For example, the dynamic equation for the temperature of the fuel channel T_f can be derived using energy balance as follows:

$$\dot{T}_f = \frac{1}{\sum_{x_f} c_{v,x_f} m_{x_f}} (H^{\mathrm{abs}}_{\mathrm{in},f} - H^{\mathrm{abs}}_{\mathrm{out},f} + Q^{\mathrm{conv}}_{\mathrm{PEN}/f} + Q^{\mathrm{conv}}_{I/f} + Q_{r,f}) \tag{5}$$

where $H^{\mathrm{abs}}_{\mathrm{in},f} - H^{\mathrm{abs}}_{\mathrm{out},f}$ accounts for the inlet and outlet absolute enthalpy difference in the fuel channel, $Q^{\mathrm{conv}}_{\mathrm{PEN}/f}$ and $Q^{\mathrm{conv}}_{I/f}$ account for the convective heat exchange between the fuel flow and its surrounding solid layers, namely, the PEN and I layers, and $Q_{r,f}$ is the energy released from the oxidation reaction in the anode. Details on each of these terms and the dynamic equations for other temperature states can be found in Ref. [1].

Finally, given the total mass and temperature in each channel, the corresponding pressure is calculated using the ideal gas law. The model of the SOFC is then obtained by integrating the dynamic equations of all the discretization units and following the flow continuity, boundary conditions, and current distribution relations.

Based on the equipotential assumption, the following relations are imposed on the discretization units:

$$U^j = U_{\mathrm{cell}}, \quad j = 1, 2, \ldots, J \tag{6}$$

$$\sum_{j=1}^{J} I^j = I_{\mathrm{tot}} \tag{7}$$

where J is the total number of discretization units, U_{cell} is the operating voltage of the cell, I^j and I_{tot} are the currents drawn from the jth unit and the whole cell, respectively.

The selection of discretization units is an important modeling parameter, which has significant impact on the model accuracy and computation load. Refined discretization grids can provide more accurate spatial profiles of the variables, such as the temperature and current density distributions, and therefore lead to improved representation of the fuel cell behaviors. However, the computation time increases drastically as the number of the discretization units increases. In this work, since the interaction of the SOFC with the CB and the GT, and not the dynamics within the SOFC, is the main focus, we use the SOFC model with a minimum of four discretization units that are shown to capture adequately the average temperature and current distribution profile [1]. This results in a 52 state SOFC dynamic model, with each unit having the states of $x_{\mathrm{CH_4}}$, $x_{\mathrm{CO_2}}$, x_{CO}, $x_{\mathrm{H_2O}}$, $x_{\mathrm{H_2}}$, $x_{\mathrm{N_2}}$, $x_{\mathrm{O_2}}$, T_f, T_a, T_{PEN}, T_{fI}, and T_{aI}, where $x_{\cdot}$ are the concentrations of the species, and T_f, T_a, T_{PEN}, T_{fI}, and T_{aI} denote the temperature in the fuel channel, air channel, PEN structure, fuel-side interconnect, and air-side interconnect, respectively.

2.2 Turbine and Compressor Model. The GT model incorporates the shaft rotational speed dynamics, the compressor and the turbine submodel. Only the shaft dynamics are considered, while the turbine and compressor are modeled using static algebraic equations. The main variables used in those models include pressure p, flow W, temperature T, and power P. Note that the

Downloaded From: http://electrochemical.asmedigitalcollection.asme.org/ on 02/18/2016 Terms of Use: http://www.asme.org/about-asme/terms-of-use

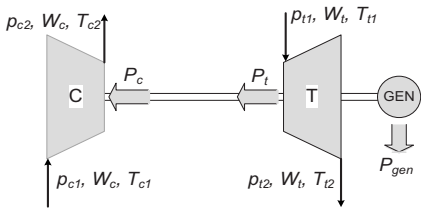

Fig. 4 Compressor, turbine, shaft, and generator schematic

subscripts denote the component (c for compressor and t for turbine) and the inlet or outlet (1 or 2, respectively). For example, T_{c2} denotes the outlet temperature of the compressor. A schematic, with all the main variables denoted at their corresponding location, is shown in Fig. 4.

2.2.1 Shaft Rotational Speed Dynamics. The turbocharger rotational dynamic behavior is determined by the power generated by the turbine, P_t (W), the power required to drive the compressor P_c (W) and the power drawn by the generator P_{gen} as

$$\frac{dN}{dt} = \frac{P_t \eta_m - P_c - P_{\text{gen}}}{\alpha N \cdot J} \tag{8}$$

where $\alpha = (2\pi/60)^2$, N is the shaft speed in rpm, and η_m is the turbine mechanical efficiency that accounts for energy losses due to friction. The turbine mechanical efficiency is considered constant and equal to a typical value of 0.95. The turbocharger inertia $J = 1.32 \times 10^{-4}$ kg m^2 is the sum of rotor inertia, compressor inertia, and turbine wheel inertia about the axis of rotation.

2.2.2 Compressor Model. Neglecting heat losses, the power required to drive the compressor (P_c) can be related to the mass flow rate through the compressor, W_c, and the total enthalpy change across the compressor from the first law of thermodynamics as

$$P_c = W_c(h_{c2} - h_{c1}) \tag{9}$$

where h_{c1} and h_{c2} are the enthalpy of the inlet and the outlet flows, respectively. Assuming that the specific heat coefficients of air do not change and by introducing the compressor isentropic efficiency, η_c, we have

$$T_{c2} = T_{c1}\left(1 + \frac{1}{\eta_c}\left(\left(\frac{p_{c2}}{p_{c1}}\right)^{(\gamma-1)/\gamma} - 1\right)\right) \tag{10}$$

$$P_c = W_c c_p^{\text{air}} T_{c1} \frac{1}{\eta_c}\left(\left(\frac{p_{c2}}{p_{c1}}\right)^{(\gamma-1)/\gamma} - 1\right) \tag{11}$$

Typically, the relation between compressor flow and efficiency to pressure ratio and compressor speed is specified in terms of nondimensional mass flow rate parameter, ϕ_c, and compressor rotational speed parameter, $\bar{N}_c$, that are defined as

$$\phi_c = \frac{W_c\sqrt{T_{c1}}}{p_{c1}} \tag{12}$$

$$\bar{N}_c = \frac{N}{\sqrt{T_{c1}}} \tag{13}$$

Details on the polynomial approximation of the compressor map can be found in Ref. [23].

2.2.3 Turbine Model. The turbine is powered by the energy of the exhaust gas. The power input to the turbine, P_t, can be obtained from the first law of thermodynamics, neglecting the heat transfer, as

$$P_t = W_t(h_{t1} - h_{t2}) \tag{14}$$

where h_{t1} and h_{t2} are the enthalpy of the inlet and the outlet turbine flows, respectively. For a given pressure ratio across the turbine, the outlet temperature can be computed assuming isentropic expansion

$$\left(\frac{T_{t1}}{T_{t2,is}}\right) = \left(\frac{p_{t1}}{p_{t2}}\right)^{(\gamma-1)/\gamma} \tag{15}$$

where $T_{t2,is}$ is the temperature of the exhaust gas leaving the turbine if the expansion was isentropic. The turbine isentropic efficiency, η_t, is introduced to calculate the turbine outlet temperature and power

$$T_{t2} = T_{t1}\left(1 - \eta_t\left(1 - \left(\frac{p_{t2}}{p_{t1}}\right)^{(\gamma-1)/\gamma}\right)\right) \tag{16}$$

$$P_t = W_t c_p T_{t1} \eta_t\left(1 - \left(\frac{p_{t2}}{p_{t1}}\right)^{(\gamma-1)/\gamma}\right) \tag{17}$$

The flow through the turbine is given as

$$W_t = \frac{A_{\text{eff}} p_{t2}}{T_{t2}}\left(\left(\frac{p_{t1}}{p_{t2}} - g + 1\right)^{2/\gamma} - \left(\frac{p_{t1}}{p_{t2}} - g + 1\right)^{(\gamma+1)/\gamma}\right)^{0.5} \tag{18}$$

where $A_{\text{eff}} = 0.07$ m^2 is the effective flow area, and $g = 0.9$ is the pressure ratio where the flow becomes zero. The isentropic efficiency is then given as a function of the blade-speed ratio U/C, defined as

$$U/C = \frac{\pi D N}{\sqrt{2 c_p T_{t1}\left(1 - \left(\frac{p_{t2}}{p_{t1}}\right)^{(\gamma-1)/\gamma}\right)}} \tag{19}$$

where D denotes the turbine blade diameter.

2.3 Catalytic Burner Model. The catalytic burner is the device where the remaining fuel from the SOFC anode is burnt with the remaining air from the SOFC cathode, in order to increase the temperature of the flow before it enters the turbine. In modeling the CB, the dynamics taken into account is the mass dynamics via the mass balance as

$$\frac{dm_{\text{CB}}}{dt} = W_{\text{ca}} + W_{\text{an}} - W_t \tag{20}$$

where W_{an} and W_{ca} are the anode and cathode outlet mass flows, respectively, and W_t is the flow through the turbine.

The temperature dynamics are expressed using the energy conservation

$$m_{\text{bed}}^{\text{CB}} c_{p,\text{bed}}^{\text{CB}} \frac{dT_{\text{CB}}}{dt} = (H_{T_{\text{CB}}}^{\text{in}} - H_{T_{\text{ref}}}^{\text{in}} - H_o^{\text{in}}) - (H_{T_{\text{CB}}}^{\text{out}} - H_{T_{\text{ref}}}^{\text{out}} - H_o^{\text{out}}) \tag{21}$$

where $H_{T_{\text{CB}}}$ and $H_{T_{\text{ref}}}$ are the enthalpies of the inlet or the outlet flow at temperatures T_{CB} and T_{ref}, respectively, while H_o is the enthalpy of formation of the inlet or outlet flow. Note that $m_{\text{bed}}^{\text{CB}}$ and $c_{p,\text{bed}}^{\text{CB}}$ are properties of the CB bed reactor and thus are considered constant.

Furthermore, the enthalpies at a given temperature T are calculated as

$$H_T = \sum_{k=1}^{k} n_k c_p^k(T) T \tag{22}$$

where n_k is the molar flow of species k, c_p^k is the specific heat of species k as a function of temperature, and T is the temperature at which the enthalpy is calculated for. In order to calculate the outlet flow composition and the outlet enthalpy $H_{T_{\text{CB}}}^{\text{out}}$, we assume that the remaining H_2 and CO are oxidized instantaneously (i.e., equilibrium reactor).

Downloaded From: http://electrochemical.asmedigitalcollection.asme.org/ on 02/18/2016 Terms of Use: http://www.asme.org/about-asme/terms-of-use

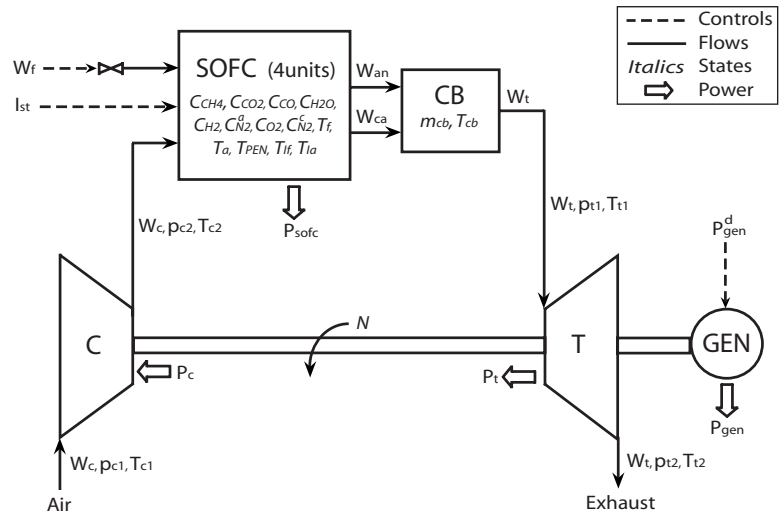

Fig. 5 Hybrid SOFC/GT schematic including inputs, controls, state variables, and parameters

The ideal gas law is used to calculate the pressure in the CB, which is then used as the inlet pressure of the compressor.

2.4 System Model. In order to integrate the submodels, the following conditions and assumptions are used.

- The compressor outlet pressure is equal to the pressure of the first SOFC discretization unit.
- The turbine inlet pressure is equal to the pressure of the catalytic burner.
- The air and fuel flow from the SOFC to the CB is dictated by the pressure difference between the last SOFC discretization unit and the CB.
- The flow out of the CB is dictated by the turbine maps, i.e., given the pressure and temperature conditions at the CB outlet, the turbine map yields the flow out of the CB and through the turbine.
- The fuel flow to the SOFC does not have any dynamics and is thus always equal to the commanded fuel flow.
- The generator load is an input to the system, which affects the shaft rotational speed through the shaft dynamics.

The system model of the hybrid SOFC/GT system has 55 state variables, of which 52 are from the 4 unit SOFC model developed in Ref. [1], 2 are from the CB, and 1 is from the GT shaft dynamics. A schematic denoting all the state variables, inputs, controls, and main variables is shown in Fig. 5. The actuators used to control the system are the fuel flow, W_f, the current drawn from the SOFC stack, I_{st}, and the generator load, P_{gen}, as shown in Fig. 5. Open loop simulations of the integrated model are shown in Sec. 3, after the optimal setpoints for the three actuators are derived by maximizing the system's efficiency.

3 Open Loop Optimization and Analysis

In this section, results on steady state optimization and open loop analysis will be shown. In order to achieve maximum system efficiency, model-based optimization is performed using the gradient algorithm to determine the setpoints for the fuel flow, the generator load, and the SOFC current for each demanded power. The analysis reveals that load following using a feedforward controller based on these optimum setpoints is not possible for the highly integrated SOFC and GT system. System shutdown is observed when a large load step is applied. Through dynamic analysis, it is shown that this phenomenon is largely attributed to the shaft rotational dynamics and the rapid increase in generator load.

3.1 Steady State Optimization. The hybrid SOFC/GT system involves multiple actuators and inputs whose setting will dictate the system operation safety and efficiency. In this section, three inputs, the fuel flow supply, the current drawn from the SOFC, and the load applied to the generator, are considered. For a given fuel flow, different combinations of currents drawn from the SOFC and loads applied to the generator will yield different net power. Note that the net power, P_{net}, of the system is defined as the sum of the power output of the fuel cell P_{SOFC} and the power output of the generator P_{gen}

$$P_{net} = P_{SOFC} + P_{gen} \tag{23}$$

In order to determine the maximum steady state net power output for a given fuel flow, the following optimization problem is solved using the developed model and gradient optimization:

$$\max_{I_{st}, P^d_{gen}, W_f} \quad (\eta_{SOFC/GT}) \quad \text{for each} \quad P_{net} \tag{24}$$

where P^d_{gen} is the generator power demand. In Eq. (24), $\eta_{SOFC/GT}$ is the efficiency of the hybrid SOFC/GT system defined as

$$\eta_{SOFC/GT} = \frac{P_{net}}{Q_{LHV_f} \cdot W_f} \tag{25}$$

where Q_{LHV_f} is the lower heating value of the fuel. By repeating the optimization problem for different net powers, the optimal steady state operation setpoints are obtained, as shown in Fig. 6, which depicts the current density to be drawn from the SOFC unit,[1] the required fuel flow, and the power delivered by the generator as functions of the net power generated by the integrated system. Note that with the given size of turbine and compressor, the optimal setpoints result in an air flow, which is five times bigger than the airflow required to support the electrochemical reaction for the amount of current drawn from the SOFC. The excess air is required for temperature control and heat removal. These setpoints can be used as static feedforward maps to schedule the actuators and power split to achieve maximum steady state efficiency for different power demands. This configuration is referred to in this work as the open loop control scheme.

3.2 Open Loop Response. Without any feedback control in place, we consider the open loop response when a demanded load power step, from P^d_{net}=20 kW to P^d_{net}=25 kW, is applied. The

[1]Note that $I_{st}=A_c \cdot i$, where A_c is the cell area.

Downloaded From: http://electrochemical.asmedigitalcollection.asme.org/ on 02/18/2016 Terms of Use: http://www.asme.org/about-asme/terms-of-use

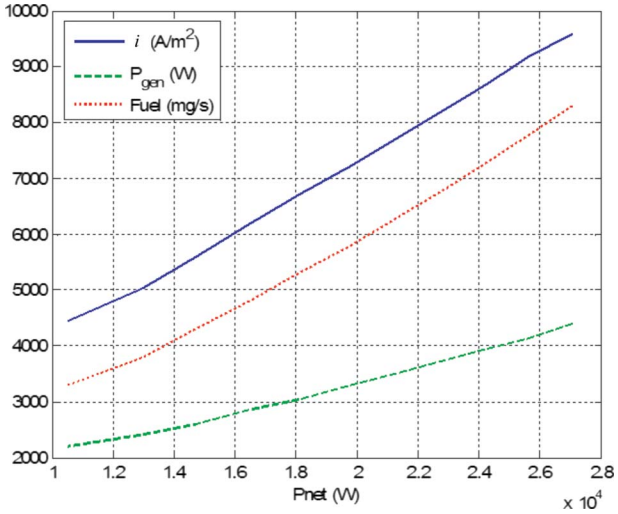

Fig. 6 Steady state optimal setpoints (FF map) for current density (i), fuel, and generator load (P_{gen}) as functions of net load

optimal input settings, identified from the optimization, are used to change the fuel flow, the current density, and the generator load from 5.8 g/s to 7.6 g/s, 7296 A/m^2 to 8946 A/m^2, and 3.30 kW to 4.05 kW, respectively, synchronized with the change in power demand. It is observed that the system shuts down (namely, the turbine shaft speed reaches zero) in about 20 s after the steps are applied. For a smaller step though, from 20 kW to 20.5 kW, the shaft is able to support the applied load, and the system reaches the desired net power after 31 s. During the 20–25 kW step, the large increase (step) in the generator load deprives the compressor from having enough power to supply the air during the transient to support the SOFC operation, causing the turbine shaft to stall and eventually the system to shut down. Therefore, open loop feedforward operation using the optimal steady state setpoints without load rate limiting or load filtering is not an option for rapid load following.

For load shedding, when a net power step down is applied, the rapid reduction in the generator load will cause a significant overshoot in air supply to the SOFC, which in turn leads to a reduction

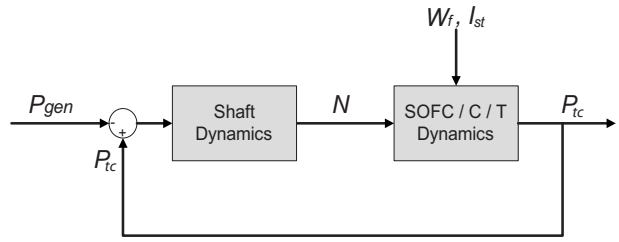

Fig. 8 Equivalent schematic of SOFC/GT system with shaft dynamics separated

in the SOFC temperature. However due to the large SOFC thermal inertial, this temperature transient happens gradually and smoothly. Thus, no transient issues for load shedding are identified.

3.3 Shutdown Dynamics Characterization. In this section, dynamic analysis reveals that the shutdown is initiated by the gas turbine, specifically its shaft dynamics. The rotational speed of the shaft N, and thus the air flow to the SOFC, is a function of the power balance on the shaft according to Eq. (8). A large load step in P_{gen}, causes $dN/dt<0$ and thus the speed to decrease. Figure 7 shows the trajectories on the (P_{tc},N) plane for the responses to a step in P_{net}^d from 20 kW to 20.5 kW and from 20 kW to 21 kW, where P_{tc} is the power of the turbine minus the power of the compressor, i.e., $P_{tc}\equiv P_t\eta_m-P_c$. For the 20–21 kW step, it can be seen that the trajectory will slide toward the lower left corner of the (P_{tc},N) plane until the system shuts down, namely $N\rightarrow 0$. Note that the initial increase in P_{tc} is due to the corresponding fuel step, which provides power almost instantaneously to the shaft. The steady state relationships between P_{tc} and N are also shown in Fig. 7, for $P_{net}=[20,20.5,21]$ kW. The steady state relationship between P_{tc} and N is determined by decoupling the shaft dynamics from the model and varying N as an input.

Given that the use of the full order model for analytic investigation of the shutdown phenomenon is prohibited due to its complexity, we attempt to develop a reduced order model to capture the effects of P_{gen}^d on the shaft rotational speed. An equivalent schematic of the SOFC/GT plant is given in Fig. 8, where the shaft dynamics are separated from the SOFC, C, and T models. To

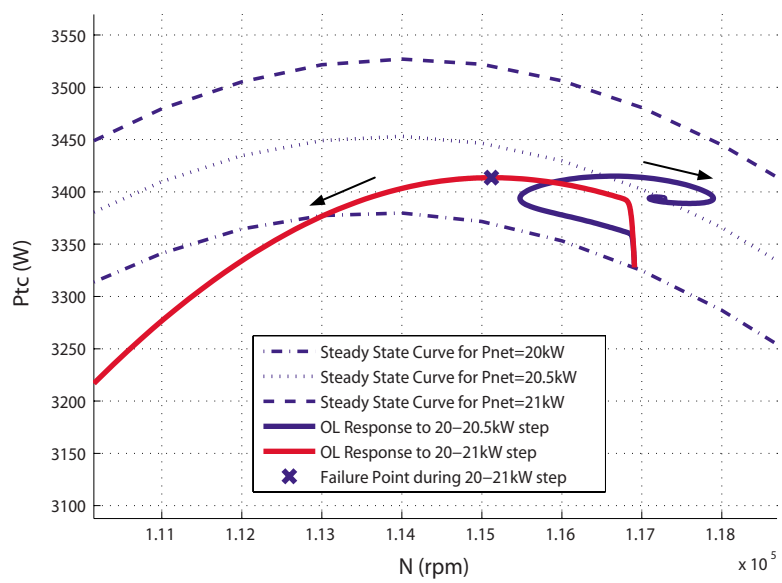

Fig. 7 System response during a 20–20.5 kW and 20–21 kW step in a P_t-P_c versus N plot

Downloaded From: http://electrochemical.asmedigitalcollection.asme.org/ on 02/18/2016 Terms of Use: http://www.asme.org/about-asme/terms-of-use

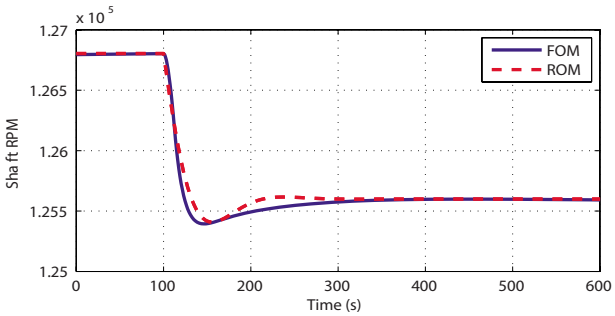

Fig. 9 Full order model (FOM) and reduced order model (ROM) shaft speed response to a 3558–3650 W step in P^d_{gen}

capture the effects of the P^d_{gen} input only, we ignore the effects of W_f and I_{st} and approximate the dynamics from N to P_{tc} with simple first order dynamics $(1/(\tau s+1))$. We know that at steady state, as shown in Fig. 7, the relationship between N and P_{tc} can be approximated by a second order polynomial of the form

$$P_{tc} = aN^2 + bN + c \tag{26}$$

with $a<0$. Multiplying the right hand side of the equation with the first order dynamics, the dynamic relationship between N and P_{tc} can be expressed as

$$\dot{P}_{tc} = \frac{a}{\tau}N^2 + \frac{b}{\tau}N + \frac{c}{\tau} - \frac{1}{\tau}P_{tc} \tag{27}$$

For a given set of inputs $(W_f, I_{\text{st}}, P^d_{\text{gen}}) = (6.2\ \text{g/s}, 7620\ \text{A/m}^2, 3558\ \text{W})$, the parameters in Eq. (27) can be identified from the full order model as

$$(a,b,c,\tau) = (-5.1\times 10^{-6},\ 1.17, -63520,\ 0.005)$$

Thus, the equivalent second order system can be expressed as

$$\begin{bmatrix} \dot{P}_{tc} \\ \dot{N} \end{bmatrix} = \begin{bmatrix} \frac{a}{\tau}N^2 + \frac{b}{\tau}N + \frac{c}{\tau} - \frac{1}{\tau}P_{tc} \\ (P_{tc} - P_{\text{gen}})/(\alpha N \cdot J) \end{bmatrix} \tag{28}$$

The response to a step from 3558 W to 3650 W in generator load is shown in Fig. 9, where the matching of the full order model (FOM) with the reduced order model (ROM) can be verified. Note that the ROM only captures the effects of P^d_{gen} in order to analyze the shutdown, while the effects of fuel and current are ignored at this point.

Also note that the second order ROM has the following two equilibrium points:

$$(N, P_{tc})_{\text{st}} = \left(\frac{-b + \sqrt{b^2 - 4a(c - P_{\text{gen}})}}{2a}, P_{\text{gen}} \right) \tag{29}$$

$$(N, P_{tc})_{\text{ust}} = \left(\frac{-b - \sqrt{b^2 - 4a(c - P_{\text{gen}})}}{2a}, P_{\text{gen}} \right) \tag{30}$$

where $(N, P_{tc})_{\text{st}}$ is a stable and $(N, P_{tc})_{\text{ust}}$ is an unstable equilibrium point.

The following theorem relates the system shutdown to the transient conditions of the system described in Eq. (28). The theorem can be used in the early detection of the shutdown phenomenon and in a control scheme as a constraint. In case the control scheme (for example a reference governor) utilizes model-based simulations to determine whether the generator load will cause shutdown, one can use this constraint to indicate the onset of shutdown and thus reduce simulation time.

THEOREM. Consider the system in Eq. (28) with state variables $x=[N\ \ P_{tc}]^T$ and input P^d_{gen} when an input step increase from P_{gen1} to P_{gen2} is applied with $x_{ss}=[N_{ss} P_{tc,ss}]^T$ being the stable equilibrium point with input P_{gen2}. If the operating point enters the following set:

$$Z = \left\{ P_{tc} < P_{tc,ss} \ \text{ and } \ N < \frac{-b - \sqrt{b^2 - 4a(c - P_{tc})}}{2a} \right\} \tag{31}$$

then

$$\lim_{t\to\infty} N = 0$$

Proof. We want to show that if $x(t) \in Z$, then $x(t)$ is outside the region of attraction of the stable equilibrium. Consider the following Lyapunov function (i.e., the distance of the operating setpoint x from the equilibrium x_{ss}):

$$V(x) = \tfrac{1}{2}(P_{tc} - P_{tc,ss})^2 + \tfrac{1}{2}(N - N_{ss})^2 \tag{32}$$

with

$$V(x) > 0, \quad \forall\, x \neq x_{ss} \tag{33}$$

$$V(x_{ss}) = 0 \tag{34}$$

$$\|x\| \to \infty \Rightarrow V(x) \to \infty \tag{35}$$

The derivative of V can be expressed as

$$\dot{V}(x) = \dot{P}_{tc}(P_{tc} - P_{tc,ss}) + \dot{N}(N - N_{ss}) \tag{36}$$

Note that $x \in Z$ implies that $\dot{V}(x) > 0$ since

$$P_{tc} < P_{tc,ss} \overset{(8)}{\rightarrow} \dot{N} < 0$$

$$N < \frac{-b - \sqrt{b^2 - 4a(c - P_{tc})}}{2a} \overset{(27)}{\rightarrow} \dot{P}_{tc} < 0$$

$$P_{tc} < P_{tc,ss} \ \text{ and } \ N < \frac{-b - \sqrt{b^2 - 4a(c - P_{tc})}}{2a} \overset{(29)}{\rightarrow} N < N_{ss}$$

Thus, the distance between the operating point and the stable equilibrium increases, and the trajectory heads away from the equilibrium. To prove the divergence of the trajectory from the stable equilibrium once the trajectory enters Z, we also need to show that

$$x(t_o) \in Z \Rightarrow x(t) \in Z \quad \forall \quad t \geq t_o \tag{37}$$

This can be verified using the quadratic form of the nonlinearity in Eq. (27) and the phase portrait of the system, shown in Fig. 10. Thus, all the points that belong in Z do not belong to the region of attraction of the stable equilibrium.

Physically this theorem says that unless the power into the shaft (P_{tc}) increases when the speed decreases, then the system has no way of stabilizing itself. If the speed drops and at the same time the energy powering the shaft drops, the speed will continue to drop until the system shuts down. The same analysis applies to the full order model.

The energy balance by integrating Eq. (8) provides insight into the possible mechanisms for avoiding shutdown

$$\underbrace{\int_0^t P_{tc} d\tau}_{E_{\text{in}}} - \underbrace{\int_0^t P_{\text{gen}} d\tau}_{E_{\text{out}}} = \underbrace{J\left(\frac{2\pi}{60}\right)^2 (N^2(t) - N_o^2)}_{\Delta E} \tag{38}$$

Note that the energy that we put into the shaft $(E_{\text{in}} = \int_0^t P_{tc} d\tau)$ minus the energy we draw from the shaft through the generator $(E_{\text{out}} = \int_0^t P_{\text{gen}} d\tau)$ is a function of the initial and current rotational speeds. From this energy balance equation (38), one can consider the following two possible solutions to mitigate shutdown:

- reduce E_{out} by filtering the generator load P_{gen} or
- increase E_{in} by adding extra fuel in the system during a transient to support the generator load

Downloaded From: http://electrochemical.asmedigitalcollection.asme.org/ on 02/18/2016 Terms of Use: http://www.asme.org/about-asme/terms-of-use

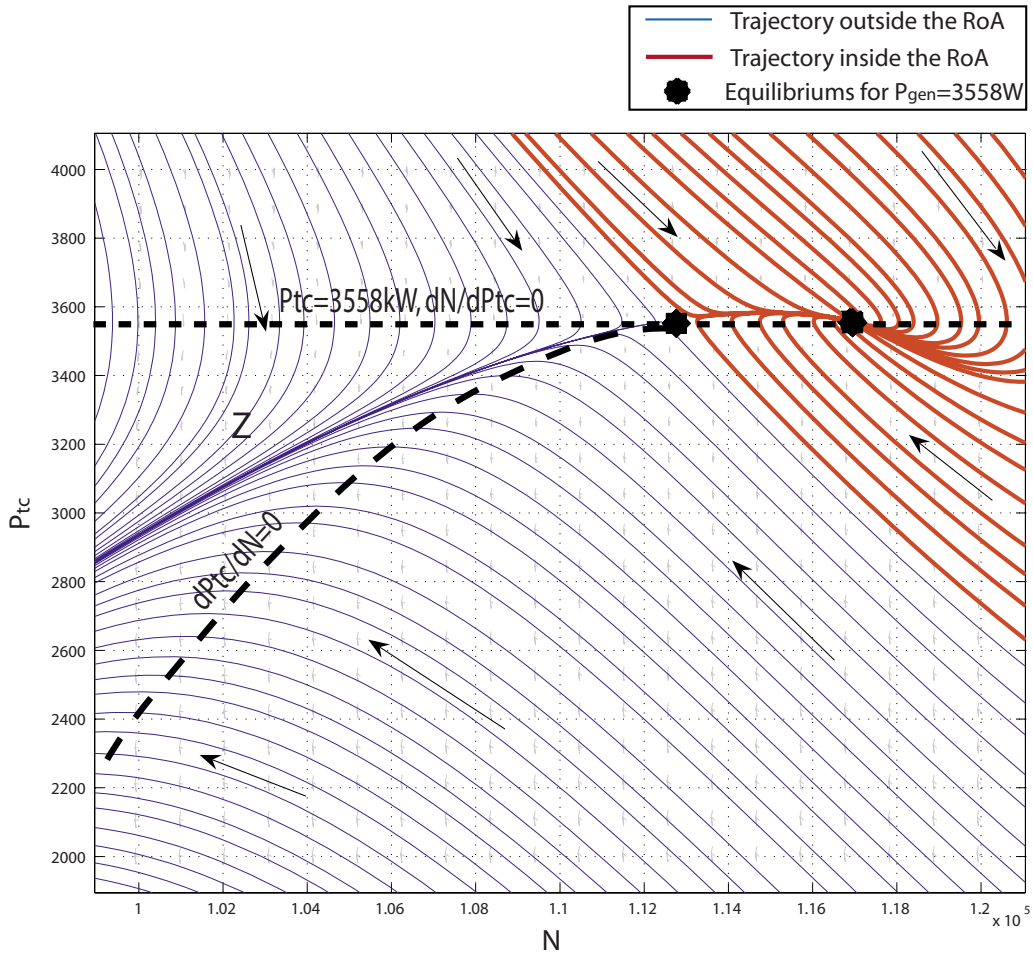

Fig. 10 Phase portrait of simplified system with state variables P_{tc} and N

The first strategy, on reducing the rate of the energy drawn from the generator, will be implemented in open loop via a generator load rate limiter and in closed loop scheme via a reference governor controller. Increasing the energy input to the shaft will be the focus of our future publication.

4 Transient Response With Rate Limiter

Given that a rapid increase in the generator load was shown to be the main cause of system shutdown, an intuitive solution is to add a rate limiter to slow down the application of P_{gen}. Multiple rate limits are examined, varying from 3.3 W/s to 6.7 W/s. From Fig. 11, one can see that system shutdown is avoided, however, the net power response will depend on the rate limit.

To understand the response shown in Fig. 11, we refer to Eq. (23). The generator load affects the net power through two paths: the direct one and the indirect one via the SOFC power

$$P_{\text{net}} = P_{\text{gen}} + P_{fc}(P_{\text{gen}}) \tag{39}$$

The second path is mainly due to the SOFC-GT coupling. Note that lower P_{gen} will lead to higher air flow being delivered to the SOFC, which results in lower temperature and lower SOFC power. From this analysis, one can see that it is critical to maximize P_{gen} to ensure fast load following.

However, with the open loop configuration the fastest rate limiter on P_{gen} that will not cause shutdown for a 20–21 kW step is 6.7 W/s. This rate limit results in a P_{net} settling time of 168 s. Note that a constant rate limiter optimized for a given step will be suboptimal for smaller steps, but insufficient to prevent shutdown for larger steps. In Sec. 5, a more elaborate feedback control scheme is proposed that guarantees stable operation and fast load following for any load step at the expense of more measurements and complex computations.

5 Reference Governor Control

In this section a feedback control scheme is presented to ensure that the system will not shut down during load transitions. Guided by the analysis of the shutdown dynamics, we propose a load governor for the generator to limit the load application whenever necessary to avoid shutdown. The controller is designed based on the reference governor approach [24], where the maximum feasible step size of the reference command is determined online through repeated simulations and optimization. The proposed control configuration is shown in Fig. 12 and explained as follows.

For a dynamic system of the form

$$\dot{x} = f(x,u) \tag{40}$$

with desired input u_d, the reference governor calculates the reference input u_{RG} such that it does not violate the constraints set for the system's response or performance. The reference command can be expressed as

$$u_{\text{RG}}(t+\delta t) = u_{\text{RG}}(t) + K(u_d(t) - u_{\text{RG}}(t)) \tag{41}$$

where $K \in [0,1]$. The value of K is determined online according to the following optimization problem formulation:

Downloaded From: http://electrochemical.asmedigitalcollection.asme.org/ on 02/18/2016 Terms of Use: http://www.asme.org/about-asme/terms-of-use

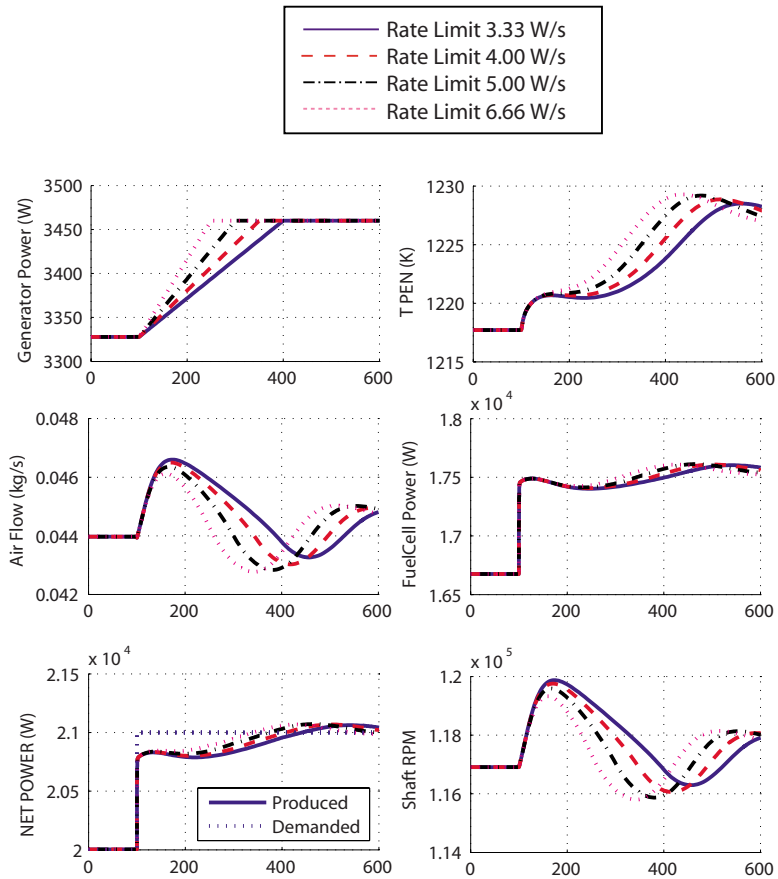

Fig. 11 Step response from 20 kW to 21 kW with various rate limiters on P^d_{gen}

$$\min_K |u_{RG} - u_d|, \quad \text{such that } O_f \text{ is satisfied} \tag{42}$$

and O_f is the set of constraints applied to the state variables of the system. The solution of Eq. (42) implies that all the constraints are satisfied, while the desired reference is tracked as close as possible.

For the hybrid SOFC/GT system, the constraint involves the system stability and can be expressed as

$$O_f = \{x \in R_A(P_{net} = u_{RG}(t))\} \tag{43}$$

where the operating point x has to belong to the region of attraction, R_A, of the equilibrium point with the current input $(u_{RG}(t))$.

DEFINITION. *Region of attraction* [25]: *let* $x = x_{ss}$ be an asymptotically stable equilibrium point for the nonlinear system

$$\dot{x} = f(x) \tag{44}$$

where $f: D \to R^n$ is a local Lipschitz and $D \subset R^n$ is a domain containing x_{ss}. Let $\phi(t;x)$ be the solution of Eq. (44) *that starts at the initial state* x at time $t=0$. The region of attraction of the equilibrium, denoted by $R_A(x_{ss})$, is defined by

$$R_A(x_{ss}) = \{x \in D | \phi(t;x) \quad \text{is defined} \quad \forall \quad t \geq 0 \quad \text{and} \quad \phi(t;x) \to x_{ss} \quad \text{as} \quad t \to \infty\}$$

For our problem, the stability of the system refers to the condition that the desired equilibrium can be reached. From the definition of the region of attraction, one can see that Eq. (43), together with the fact that each equilibrium corresponding to a given u_d is locally stable, will guarantee that no system shutdown occurs, and therefore the stability condition of the system can be satisfied.

The optimization problem posed in Eq. (42) is solved using the bisection algorithm outlined below. The model is simulated forward in time over a given horizon. If the constraints are violated at any time during the simulated period, the value of K is reduced and the simulation is reinitiated. If the constraints are satisfied for the entire simulated trajectory, the value of the reference command is increased by the bisection algorithm until it converges [24]. To describe the algorithm formally, let us first define $h(K)$ as

$$h(K) = \begin{cases} 1 & \text{if } O_f \text{ is satisfied} \\ 0 & \text{if } O_f \text{ is not satisfied} \end{cases} \tag{45}$$

Given an interval $[K_l, K_r]$ with left limit (i.e., lower bound) K_l and right limit (i.e., higher bound) K_r, the bisection algorithm is summarized as

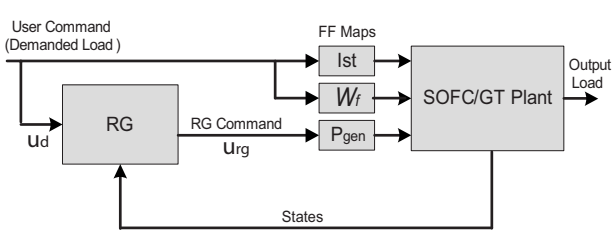

Fig. 12 Closed loop schematic with reference governor (RG) control

Downloaded From: http://electrochemical.asmedigitalcollection.asme.org/ on 02/18/2016 Terms of Use: http://www.asme.org/about-asme/terms-of-use

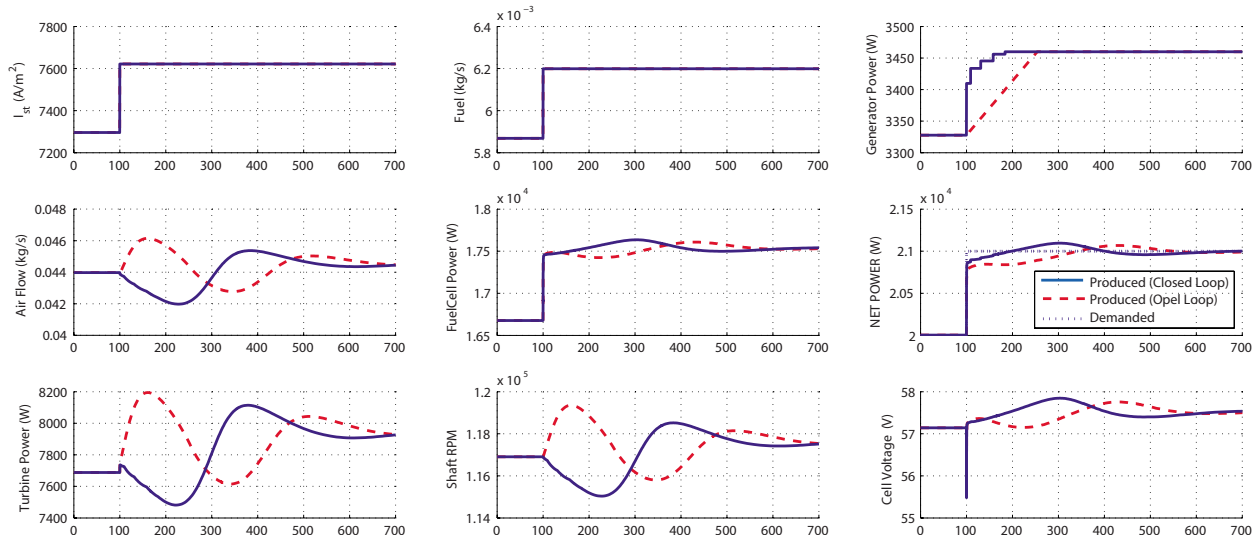

Fig. 13 Open and closed loop 20–21 kW step response

```
while |K_r − K_l| > ε
  K_m = (K_r + K_l)/2
  If h(K_l)·h(K_m) > 0
    K_l = K_m
  Else
    K_r = K_m
  end if
end while
```

where ϵ is set to 0.01 in order to prevent the optimization from running indefinitely. Note that the initial values of K_r and K_l are set as $K_l=0$ and $K_r=1$. Furthermore, we have $h(0)=1$.

The open loop response with the fastest possible rate limiter and the closed loop system responses to a 20–21 kW step in demanded load are shown in Fig. 13. The filtering of the generator load command applied by the reference governor prevents shutdown of the system. The drawback of this load governor, implemented using a conventional method, is that the computational time involved and the measurements required make it infeasible for real-time implementation. The full state variable information is needed to initiate each simulation and to provide the state feedback. An alternative reference governor implementation, which leads to substantially lower computational demand and does not require full state measurement, will be the focus of our future work [23].

6 Summary and Conclusions

In this paper the efficiency and the transient operation of a hybrid solid oxide fuel cell and gas turbine system are analyzed. A nonlinear control oriented model is developed and used initially for defining, via optimization, the fuel, current, and generator load setpoints that yield the highest system efficiency. However, these setpoints can cause system shutdown when large and fast transitions are attempted. The shutdown phenomenon is analyzed and the fast coupling between the fuel cell and the gas turbine is identified as the main cause for the shutdown phenomenon.

To mitigate the shutdown problems associated with the open loop operation, a reference governor control scheme was developed and implemented to modify the application of the generator load. Slowing down the energy drawn from the generator allows more power to be delivered to the shaft, thereby preventing a large rotational speed drop of the shaft. The reference governor achieves the constraint enforcement without compromising tracking performance by using online optimization. The drawback of applying this reference governor is the high computational requirements and the need for full state feedback that make it ineffective for real-time implementation. An alternative reference governor that solves the transient optimization problem without resorting to repeated simulations is currently being developed and will be presented in our future work.

Acknowledgment

This work is supported by the ONR under U.S. Navy Contract Nos. N00014-06-1-0209, NSF ECS-0501248, and CMS-0625610.

Nomenclature

Symbols

A_{eff} = turbine effective flow area (m^2)
A_c = cell area (m^2)
$c_{(\cdot)}$ = concentration of species $(\cdot)$ (mol)
c_P = heat capacity (J/kg K)
H^{abs} = absolute enthalpy (J/kg)
i = current density (A/m^2)
I_{st} = stack current, input (A)
J = shaft inertia (kg m^2)
k = orifice coefficient (kg/s $Pa^{0.5}$)
m = mass (kg)
M = molar weight (kg/mol)
N = shaft rotational speed (rpm)
$p_{(\cdot)}$ = pressure of $(\cdot)$ (Pa)
P_{fc} = fuel cell power, output (W)
P_{gen} = generator load (W)
P_{gen}^d = generator desired load (W)
P_{net} = net power output (W)
P_{net}^d = net power demand (W)
P_c = compressor power (W)
P_t = turbine power (W)
Q_{LHV_f} = lower heating value of the fuel (J/kg)
R = universal gas constant (J/K mol)
T = temperature (K)
U = voltage (V)
V = volume (m^3)
W = flow (kg/s)
$x_{(\cdot)}$ = molar fraction of species $(\cdot)$
η_{hc} = compressor isentropic efficiency
η_{ht} = turbine isentropic efficiency

Downloaded From: http://electrochemical.asmedigitalcollection.asme.org/ on 02/18/2016 Terms of Use: http://www.asme.org/about-asme/terms-of-use

$\eta_{SOFC/GT}$ = SOFC/GT system efficiency
η^j_{ohm} = ohmic loss of unit j (V)
η^j_{act} = activation loss of unit j (V)
η^j_{con} = concentration loss of unit j (V)

References

[1] Xi, H., 2007, "Dynamic Modeling and Control of Planar SOFC Power Systems," Ph.D. thesis, University of Michigan, Ann Arbor, MI.

[2] Tsourapas, V., Sun, J., and Stefanopoulou, A., 2004, "Modeling and Dynamics of a Fuel Cell Combined Heat Power System for Marine Applications," IASME Transactions, **2**(1), pp. 287–293.

[3] Tsourapas, V., Stefanopoulou, A., and Sun, J., 2007, "Model-Based Control of an Integrated Fuel Cell and Fuel Processor With Exhaust Heat Recirculation," IEEE Trans. Control Syst. Technol., **15**, pp. 233–245.

[4] Lundberg, W. L., Veyo, S. E., and Moeckel, M. D., 2003, "A high-Efficiency Solid Oxide Fuel Cell Hybrid Power System Using the Mercury 50 Advanced Turbine Systems Gas Turbine," ASME J. Eng. Gas Turbines Power, **125**, pp. 51–57.

[5] Kuchonthara, P., Bhattacharya, S., and Tsutsumi, A., 2003, "Energy Recuperation in Solid Oxide Fuel Cell (SOFC) and Gas Turbine (GT) Combined System," J. Power Sources, **117**, pp. 7–13.

[6] Kimijima, S., and Kasagi, N., 2005, "Cycle Analysis of Micro Gas Turbine Molten Carbonate Fuel Cell Hybrid System," JSME Int. J., Ser. B, **48**, pp. 65–74.

[7] Silveira, J., and Gomes, L., 1999, "Fuel Cell Cogeneration System: A Case of Technoeconomic Analysis," Renewable Sustainable Energy Rev., **3**, pp. 233–242.

[8] Yi, Y., Rao, A. D., Brouwer, J., and Samuelsen, G. S., 2004, "Analysis and Optimization of a Solid Oxide Fuel Cell and Intercooled Gas Turbine (SOFC-ICGT) Hybrid Cycle," J. Power Sources, **132**, pp. 77–85.

[9] Yang, W., Park, S., Kim, T., Kim, J., Sohn, J., and Ro, S., 2006, "Design Performance Analysis of Pressurized Solid Oxide Fuel Cell/Gas Turbine Hybrid Systems Considering Temperature Constraints," J. Power Sources, **160**, pp. 462–473.

[10] Massardo, A. F., and Lubelli, F., 2000, "Internal Reforming Solid Oxide Fuel Cell-Gas Turbine Combined Cycles (IRSOFC-GT): Part A—Cell Model and Cycle Thermodynamic Analysis," ASME J. Eng. Gas Turbines Power, **122**, pp. 27–35.

[11] Uechi, H., Kimijima, S., and Kasagi, N., 2004, "Cycle Analysis of Gas Turbine-Fuel Cell Cycle Hybrid Micro Generation System," ASME J. Eng. Gas Turbines Power, **126**, pp. 755–762.

[12] Palsson, J., Selimovic, A., and Sjunnesson, L., 2000, "Combined Solid Oxide Fuel Cell and Gas Turbine Systems for Efficient Power and Heat Generation," J. Power Sources, **86**, pp. 442–448.

[13] Song, T. W., Sohna, J. L., Kim, T. S., and Ro, S. T., 2006, "Performance Characteristics of a MW-Class SOFC/GT Hybrid System Based on a Commercially Available Gas Turbine," J. Power Sources, **158**, pp. 361–367.

[14] Chung, T.-D., Chyou, Y.-P., Hong, W.-T., Cheng, Y.-N., and Lin, K.-F., 2007, "Influence of Energy Recuperation on the Efficiency of a Solid Oxide Fuel Cell Power System," Energy Fuels, **21**, pp. 314–321.

[15] Lokurlu, A., Grube, T., Hohlein, B., and Stolten, D., 2003, "Fuel Cells for Mobile and Stationary Applications—Cost Analysis for Combined Heat and Power Stations on the Basis of Fuel Cells," Int. J. Hydrogen Energy, **28**, pp. 703–711.

[16] Au, S. F., McPhail, S. J., Woudstra, N., and Hemmes, K., 2003, "The Influence of Operating Temperature on the Efficiency of a Combined Heat and Power Fuel Cell Plant," J. Power Sources, **122**, pp. 37–46.

[17] Murshed, A. M., Huang, B., and Nandakumar, K., 2007, "Control Relevant Modeling of Planer Solid Oxide Fuel Cell System," J. Power Sources, **163**, pp. 830–845.

[18] Wang, X., Huang, B., and Chen, T., 2007, "Data-Driven Predictive Control for Solid Oxide Fuel Cells," J. Process Control, **17**, pp. 103–114.

[19] Roberts, R. A., and Brouwer, J., 2006, "Dynamic Simulation of a Pressurized 220 kW Solid Oxide Fuel-Cell Gas-Turbine Hybrid System: Modeled Performance Compared to Measured Results," J. Power Sources, **3**, pp. 18–25.

[20] Wächter, C., Lunderstädt, R., and Joos, F., 2006, "Dynamic Model of a Pressurized SOFC/Gas Turbine Hybrid Power Plant for the Development of Control Concepts," ASME J. Fuel Cell Sci. Technol., **3**, pp. 271–279.

[21] Stiller, C., Thorud, B., and Bolland, O., 2006, "Safe Dynamic Operation of a Simple SOFC/GT Hybrid System," ASME J. Eng. Gas Turbines Power, **128**, pp. 551–559.

[22] Stiller, C., Thorud, B., Bolland, O., Kandepu, R., and Imsland, L., 2006, "Control Strategy for a Solid Oxide Fuel Cell and Gas Turbine Hybrid System," J. Power Sources, **158**, pp. 303–315.

[23] Tsourapas, V., 2007, "Control Analysis of Integrated Fuel Cell Systems With Energy Recuperation Devices," Ph.D. thesis, University of Michigan, Ann Arbor, MI.

[24] Sun, J., and Kolmanovsky, I., 2005, "A Robust Load Governor for Fuel Cell Oxygen Starvation Protection," IEEE Trans. Control Syst. Technol., **13**, pp. 911–920.

[25] Khalil, H., 2002, *Nonlinear Systems*, 3rd ed., Prentice-Hall, Englewood Cliffs, NJ.

Downloaded From: http://electrochemical.asmedigitalcollection.asme.org/ on 02/18/2016 Terms of Use: http://www.asme.org/about-asme/terms-of-use